Steel and Composite Structures, Vol. 9, No. 3 (2009) 275-301
DOI: http://dx.doi.org/10.12989/scs.2009.9.3.275

Thin-walled composite steel-concrete beams subjected to skew bending and torsion

Francesca Giussani* and Franco Mola†

Department of Structural Engineering, Milan University of Technology (Politecnico), P.za L. da Vinci, 32, 20133 Milan, Italy

(Received January 11, 2008, Accepted March 5, 2009)

Abstract. The long-term behaviour of simply supported composite steel-concrete beams with deformable connectors subjected to skew bending and torsion is presented. The problem is dealt with by recurring to the displacement method, assuming the bending and torsional curvatures and the longitudinal deformations of each sectional part as unknowns and obtaining a system of differential and integro-differential equations. Some solving methods are presented, in order to obtain exact and approximate solutions and evaluate the precision of the approximate ones. A case study is then presented. For the sake of clearness, the responses of the composite beam under loads applied in different directions are studied separately, in order to correctly evaluate the effects of each load condition.

Keywords : creep; composite steel-concrete beams; deformable connectors; skew bending; torsion; thin-walled section.

1. Introduction

In the last decades, many interesting works regarding the long-term behaviour of composite steel-concrete beams with flexible shear connectors have been performed, referring to straight structural elements subjected to uniaxial bending. In order to correctly take into account the slip between concrete slab and steel beam, composite beams are generally studied recurring to the force method, taking the interaction forces developing at steel-concrete interface as unknowns, as it was firstly introduced in the elastic domain by Newmark, *et al.* in 1951 and successively extended to the viscoelastic domain (Bradford and Gilbert 1992, Mola 1994, Mola and Gatti 1996, Amadio and Fragiacomo 1997, Mola and Giussani 2003, Giussani 2004, Ayoub 2005). In the last years, the finite elements method has been largely employed in this field. In particular, Ayoub and Filippou (2000) proposed an inelastic beam element for the analysis of steel-concrete girders with partial composite action derived from a two-field mixed formulation; Kwak and Seo (2002) formulated a numerical model based on continuous analytical solutions of force equilibrium equations and strain compatibility conditions at each node, with an assumption of piecewise linear distribution of the bending moment; Limkatanyu and Spacone (2002) presented three reinforced concrete frame elements with bond slip between the reinforcing bars and the concrete, for

* Corresponding Author, Email: francesca.giussani@polimi.it
† Professor, Email: mola@stru.polimi.it

the displacement-based, the force-based, and the Hellinger–Reissner mixed formulations; Dall'Asta and Zona (2004) developed a three-field mixed beam element for the non-linear analysis of composite beams with deformable shear connection; Virtuoso and Vieira (2004) proposed a finite element model based on the internal forces approximation, considering the non-linear behaviour of the connection between the steel girder and the concrete flange, the non-linear behaviour of concrete subjected to cracking in the zones of negative moment and the viscoelastic behaviour of concrete. In similar way, the uniaxial finite element model proposed by Fragiacomo, *et al*. (2004) includes connection flexibility, rheological phenomena of concrete and nonlinear behaviour of component materials.

Anyhow, in modern bridge design, composite steel-concrete beams present very different typologies of structural forms (Nakamura, *et al*. 2002) and are frequently used in the presence of complex static or geometrical schemes, such as continuous, curved beams or beams with non-symmetric sections. In these cases, the beams are subjected to skew bending and torsion. Many studies have been performed regarding the elastic behaviour of composite box girder bridges under torsional actions. Chapman, *et al*. (1971) investigated the structural behaviour of composite box girders by means of the theory of the torsion of un-deforming sections, the beam on elastic foundation analogy for deforming sections and the finite element method, by neglecting any buckling and inelasticity phenomenon. De Miranda (1961) presented a wide description of torsional behaviour of composite steel-concrete bridge beams, considering open thin-walled sections, with or without diaphragms, and box girders. Some interesting experimental campaigns have been carried out on eccentrically loaded straight multi-cell box bridges by Ng, *et al*. (1993). Referring to beams subjected to bi-axial bending, a model that calculates both short- and long-term behaviour of reinforced, prestressed and composite beams was proposed by Rodriguez-Gutierrez and Aristizabal-Ochoa (2007), by assuming perfect bond between the sectional elements.

A number of interesting works has been devoted to the study of the elastic and ultimate behaviour of curved composite steel-concrete bridges: Colville (1973) performed some experimental tests on simply supported curved composite beams, giving suggestions about the design of shear connectors. Some years later, by means of a parametric analysis performed with three-dimensional finite elements, Turkstra and Fam (1978) demonstrated the importance of warping and distorsional stresses in relation to the longitudinal normal bending stresses derived from curved beam theory. Simo and Vu-Quoc (1991) developed a non-linear 3D model incorporating shear and torsion-warping deformation; Sennah and Kennedy (1999) investigated on multi-cell box bridges, while Thevendran, *et al*. (2000) focused their attention on curved bridge decks incorporating an I girder collaborating with a concrete slab subjected to a concentrated load at mid-span; this in order to test the accuracy of finite element programs in describing the elastic behaviour of these structural arrangements, such as the one developed in Thevendran, *et al*. (1999). Topkaya and Williamson (2003) and Kim and Yoo (2006a) performed finite element analyses on curved steel girders before the construction of the concrete deck able to form a closed section. The ultimate strengths of composite box girders subjected to bending and torsion has been investigated by Kim and Yoo (2006b) by means of three-dimensional finite element analyses.

As presented in Giussani and Mola (2009), referring to continuous composite beams subjected to uniaxial bending, and in Giussani (2004), the need of extending the analysis to the viscoelastic domain and the need of describing the effects due to connector deformability make it more feasible to investigate the long-term behaviour of composite beams subjected to skew bending and torsion by means of the displacement method, assuming the bending and torsional curvatures and the longitudinal deformations of each sectional part as unknown. In this way, the problem leads to a system of integro-differential equations. Furthermore, regarding the kinematic aspects, the hypotheses concerning Vlasov's theory

(Vlasov 1962) of open thin-walled sections are assumed, taking also the relative longitudinal slip developing at the steel-concrete interface into account. The assumption of rigid transverse sections allows to express the geometrical law governing the longitudinal strains by means of four parameters of generalised sectional deformations, to which n_s parameters related to the longitudinal deformations of the n_s steel parts mutually connected to the concrete slab by means of deformable steel studs have to be added.

If adequate boundary conditions are provided, the solution can be obtained by means of the Fourier series expansion, by splitting the problem in two sub-problems, the first related to space variables and the second involving the time evolution. In a more general way, the use of the finite difference method as regards the space domain and of numerical methods, such as the rule of trapezia, for treating the time integrals can be adopted when more complex arrangements of boundary conditions have to be dealt with. In any case, interesting approximate solutions can be obtained, by introducing an algebraic law for the long-term behaviour of concrete.

2. The formulation of the problem

Let us consider the composite structure with the transverse section represented in Fig. 1. The structure is assumed as prismatic and the section consists in the concrete element "c" interacting with any number n_s of steel elements "s_i", connected by n_s elastic connection devices. The considered structure can be subjected to static loads, generically distributed along the beam axis, and imposed sectional deformations, such as shrinkage or thermal actions.

The torsional behaviour of composite steel–concrete beams can be investigated by adopting Vlasov's theory of open thin-walled sections and assuming the following hypotheses which allow to identify the sections with their mean profiles

- the transverse section is rigid in its plane;
- the shear deformation of the mean surface can be neglected.

Furthermore, it is assumed that

- shear connections between the slab and the beams are smeared along the length of the beams and

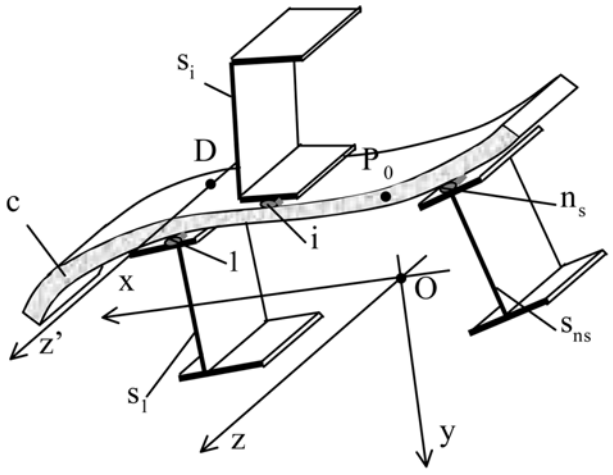

Fig. 1 Transverse section

allow only a longitudinal slip at the interface between steel and concrete elements;
- the distributions of strains throughout the depth of the slab and the beams are linear;
- the section is open.

Steel beams and steel connectors have linear elastic behaviours, while a linear visco-elastic law is adopted for concrete slab, according to Mc Henry superposition principle (McHenry 1943), as indicated in the following relationships

$$\sigma_s^{(i)}(\ell, z, t) = E_s[\varepsilon_s^{(i)}(\ell, z, t) - \bar{\varepsilon}_s^{(i)}(\ell, t)] \tag{1}$$

$$\sigma_c(\ell, z, t) = \int_0^t E_{c0} d[\varepsilon_c(\ell, z, t') - \bar{\varepsilon}_c(\ell, t')]\rho(t, t') \tag{2}$$

$$q^{(i)}(z, t) = k_{ch}^{(i)} u_{ch}^{(i)}(z, t) \tag{3}$$

where ℓ is the abscissa along the mean profile of the section, E_s is the elastic modulus of steel beam, $\rho(t, t') = R(t, t')/E_{c0}$, E_{c0}, $R(t, t')$, E_{c0}, $R(t,t')$ are respectively the reference elastic modulus and the relaxation function of concrete slab, $\bar{\varepsilon}_s^{(i)}(\ell, t)$, $\bar{\varepsilon}_c^{(i)}(\ell, t)$ are the deformations imposed respectively in steel beam and concrete slab. $k_{ch}^{(i)}$ is the elastic stiffness of the i-th connector, $u_{ch}^{(i)}$ and $q^{(i)}$ are respectively the slip and the shear flow at the i-th steel-concrete interface.

Referring to the cross section represented in Fig. 1 and neglecting the shear deformation of the mean surface (Vlasov 1962, Kolbrunner and Basler 1969), the longitudinal deformations of the concrete slab and of the steel beams can be expressed as

$$\begin{aligned} \varepsilon_c(\ell, z, t) &= \Psi_{1c}(z, t) - x(\ell)\Psi_2(z, t) - y(\ell)\Psi_3(z, t) - \omega(\ell)\Psi_4(z, t) \\ \varepsilon_s^{(i)}(\ell, z, t) &= \Psi_{1s}^{(i)}(z, t) - x(\ell)\Psi_2(z, t) - y(\ell)\Psi_3(z, t) - \omega(\ell)\Psi_4(z, t);\ i = \ell, \ldots, n_s \end{aligned} \tag{4}$$

where coordinates x, y are expressed with respect to the reference axes origin, ω is the sectorial area of the section evaluated with respect to the shear centre D and having its origin in the pole P_0; Ψ_{1c}, $\Psi_{1s}^{(i)}$ are the longitudinal strains of the concrete slab and of the i-th steel element, evaluated in the origin of the axes, Ψ_2, Ψ_3 are the flexural curvatures of the section respectively in the z-x and x-y planes and Ψ_4 is the torsional curvature of the section.

The compatibility conditions at the i-th connection point can be expressed according to the following equation

$$\varepsilon_c(\ell_i, z, t) = \varepsilon_s(\ell_i, z, t) - \varepsilon_{ch}^{(i)}(z, t), \quad i = 1, \ldots, n_s \tag{5}$$

where $\varepsilon_c(\ell_i,z,t)$, $\varepsilon_s(\ell_i,z,t)$ are the strains of the concrete and steel fibres corresponding to the i-th connection, while $\varepsilon_{ch}^{(i)}(z, t)$ is the strain of the i-th connection device, which can be expressed as a function of the shear flow

$$\varepsilon_{ch}^{(i)}(z, t) = \frac{\partial u_{ch}^{(i)}(z, t)}{\partial z} = \frac{\partial q^{(i)}(z, t)}{\partial z} \frac{\ell}{k_{ch}^{(i)}} \tag{6}$$

The shear flow can be evaluated from the equilibrium of the infinitesimal element having height $d\ell$ and length dz, as shown in Fig. 2.

Neglecting the infinitesimal terms of second order, the equilibrium condition requires that

$$\frac{\partial \sigma_s(\ell, z, t)}{\partial z} b(\ell) = -\frac{\partial [\tau_{z\ell}(\ell, z, t) b(\ell)]}{\partial \ell} \tag{7}$$

Consequently, the shear flow $q(\ell, z, t) = \tau_{z\ell}(\ell, z, t) b(\ell)$ at abscissa ℓ can be expressed as

$$q(\ell, z, t) = -\int_{\ell} b(\tilde{\ell}) \frac{\partial \sigma_z(\tilde{\ell}, z, t)}{\partial z} d\tilde{\ell} + C \tag{8}$$

where $C = 0$ as the shear flow vanishes at $\ell = \ell_{inf}$.

By introducing the constitutive law (1) of the steel beams and the second of Eq. (4) in Eq. (8), referring to the i-th steel beam, we derive

$$q^{(i)}(\ell, z, t) = E_s \left[I^{(i)}_{sr_1 r_1}(\ell) \Psi^{(i)}_{1s}(z, t) - \sum_{j=2}^{4} I^{(i)}_{sr_1 r_j}(\ell) \Psi'_j(z, t) \right] \tag{9}$$

where the apex indicates the derivative with respect to z and

$$I^{(i)}_{sr_1 r_j}(\ell) = \int_{\ell^{(i)}_{inf}}^{\ell^{(i)}} b(\ell) r_1(\ell) r_j(\ell) d\ell, \quad j = 1, \ldots, 4 \tag{10}$$

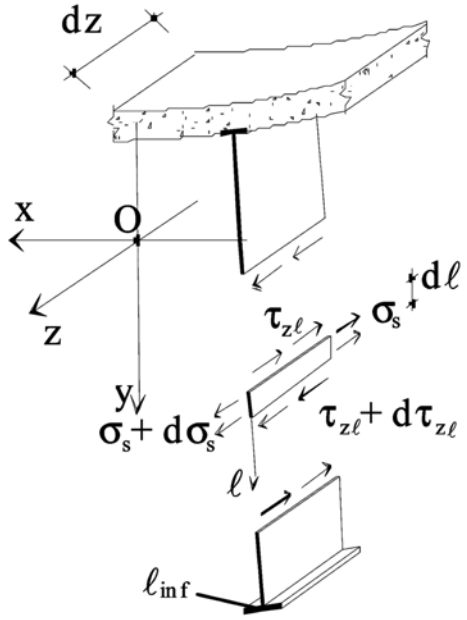

Fig. 2 Shear flow

in which r_j is the j-th component of coordinate vector $\underline{r}^T(\ell) = [1\ x(\ell)\ y(\ell)\ \omega(\ell)]$. Eq. (9) allows to determine the shear flow acting in the i-th steel element of the section at the abscissa ℓ. Hence, the shear flow at the i-th steel-concrete interface can be immediately obtained by evaluating Eq. (9) at $\ell^{(i)} = \ell_{sup}^{(i)}$, as represented in Fig. 3. Eq. (6) becomes

$$\varepsilon_{ch}^{(i)}(z,t) = \frac{E_s}{k_{ch}^{(i)}}[A_s^{(i)}\Psi_{ls}''^{(i)}(z,t) - S_{sx}^{(i)}\Psi_2''(z,t) - S_{sy}^{(i)}\Psi_3''(z,t) - S_{s\omega}^{(i)}\Psi_4''(z,t)] \tag{11}$$

where $A_s^{(i)} = I_{sr_1r_1}^{(i)}$, $S_{sx}^{(i)} = I_{sr_1r_2}^{(i)}$, $S_{sy}^{(i)} = I_{sr_1r_3}^{(i)}$, $S_{s\omega}^{(i)} = I_{sr_1r_4}^{(i)}$ are respectively the area and the static moments of the i-th steel element, $I_{sr_1r_j}^{(i)} = \int_{\ell_s^{(i)}} b(\ell) r_1(\ell) r_j(\ell) d\ell$ and $\ell_s^{(i)}$ represents the whole profile of the i-th steel beam. Introducing Eqs. (4), (11) in Eq. (5), we derive

$$\Psi_{1c}(z,t) = \Psi_{ls}^{(i)}(z,t) - \frac{E_s}{k_{ch}^{(i)}}[A_s^{(i)}\Psi_{ls}''^{(i)}(z,t) - S_{sx}^{(i)}\Psi_2''(z,t) - S_{sy}^{(i)}\Psi_3''(z,t) - S_{s\omega}^{(i)}\Psi_4''(z,t)],\ i = 1,\ldots,n_s \tag{12}$$

Eq. (12) represents a system of n_s compatibility equations involving $n_s + 4$ unknowns, i.e. the $n_s + 1$ longitudinal deformations Ψ_{1c}, $\Psi_{ls}^{(i)}$, the two flexural curvatures Ψ_2, Ψ_3 and the torsional curvature Ψ_4.

Let us now introduce vectors $\underline{\Psi}^T = [\Psi_{1c} - \Psi_2 - \Psi_3 - \Psi_4]$, $\underline{\Psi}_{ls}^T = [\Psi_{ls}^{(1)}\ \Psi_{ls}^{(2)}\ \ldots\ \Psi_{ls}^{(n_s)}]$ and matrices $\underline{\underline{\mu}} = (n_s,4)$, $\underline{\underline{\nu}} = (n_s,4)$, $\underline{\underline{\lambda}} = (n_s,n_s)$, defined as

$$\begin{aligned}
&\mu_{i,1} = 1, \quad \mu_{i,j} = 0 && j = 2,3,4\\
&\nu_{i,1} = 0, \quad \nu_{i,j} = \frac{E_s I_{sr_1r_j}^{(i)}}{k_{ch}^{(i)}} && i = 1,\ldots,n_s\\
&\lambda_{i,k} = 0, \quad \lambda_{i,i} = \frac{E_s A_s^{(i)}}{k_{ch}^{(i)}} && k = 1,\ldots,n_s \neq i
\end{aligned} \tag{13}$$

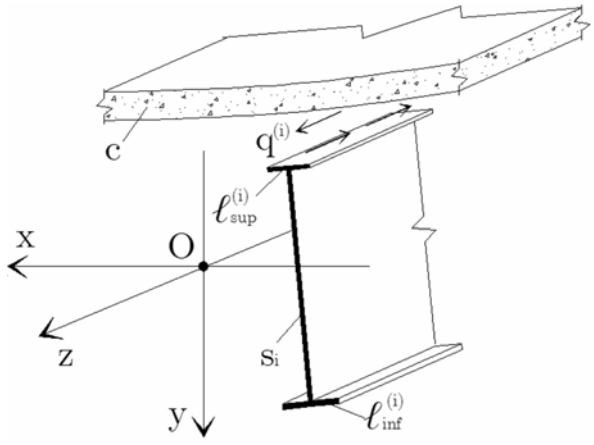

Fig. 3 Shear flow at the i-th connection device

Thus, compatibility Eq. (12) can be written in the matrix form

$$\underline{\nu}\underline{\Psi}''(z,t) + \underline{\underline{\mu}}\underline{\Psi}(z,t) = -\underline{\underline{\lambda}}\underline{\Psi}''_{ls}(z,t) + \underline{\Psi}_{ls}(z,t) \tag{14}$$

Introducing the vector of internal actions $\underline{Q}^T(z,t) = [N(z,t) - M_x(z,t)\ M_y(z,t)\ M_\omega(z,t)]$, as represented in Fig. 4, equilibrium equations assume the following expression

$$\underline{Q}(z,t) = \int_{\ell_c} \sigma_c(\ell, z, t)\underline{r}(\ell)b(\ell)d\ell + \sum_{i=1}^{n_s} \int_{\ell_s^{(i)}} \sigma_s^i(\ell, z, t)\underline{r}(\ell)b(\ell)d\ell \tag{15}$$

where ℓ_c represents the whole profile of concrete slab.

Introducing the constitutive laws (1), (2) and the kinematic relationships (4) in Eq. (15), and integrating over the whole profiles of concrete slab and steel beams, the equilibrium equations can be expressed in the following matrix form

$$\int_0^t [\underline{\underline{B}}_{c0}\rho(t,t') + \underline{\underline{B}}_s^*]d\underline{\Psi}(z,t') + \underline{\underline{C}}_s\underline{\Psi}_{ls}(z,t) = \underline{Q}(z,t) + \int_0^t d\underline{\overline{Q}}_c(t')\rho(t,t') + \underline{\overline{Q}}_s(t) \tag{16}$$

having introduced matrices $\underline{\underline{B}}_{c0} = (4,4)$, $\underline{\underline{B}}_s^* = (4,4)$, $\underline{\underline{C}}_s = (4,n_s)$, defined as

$$B_{c0i,j} = E_{c0}I_{cr_ir_j};\ I_{cr_ir_j} = \int_{\ell_c} b(\ell)r_i(\ell)r_j(\ell)d\ell\ ;\ i,j = 1,\ldots,4$$

$$B^*_{si,1} = 0\ ;\ B^*_{si,j} = E_sI_{sr_ir_j}\ ,\ I_{sr_ir_j} = \sum_{k=1}^{n_s} I^{(k)}_{sr_ir_j}\ ;\ i = 1,\ldots,4\ ;\ j = 2,3,4$$

$$C_{si,k} = E_sI^{(k)}_{s\ r_1r_i}\ ;\ i = 1,\ldots,4;\ k = 1,\ldots,n_s \tag{17}$$

and vectors $\underline{\overline{Q}}_c(t)$, $\underline{\overline{Q}}_s(t)$ including the contributions of the deformations imposed on concrete slab and

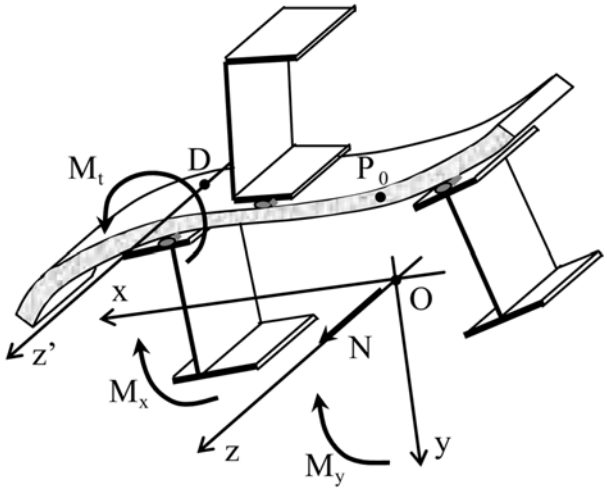

Fig. 4 Internal actions

steel beam, according to the following relationships

$$\overline{\underline{Q}}_c(t) = \int_{\ell_c} E_{c0} d\bar{\varepsilon}_c(\ell, t) r(\ell) b(\ell) d\ell \ , \quad \overline{\underline{Q}}_s(t) = \sum_{i=1}^{n_s} \int_{\ell_s^{(i)}} E_s d\bar{\varepsilon}_s^{(i)}(\ell, t) \underline{r}(\ell) b(\ell) d\ell \tag{18}$$

Eq. (16) represents the time relationship between the normal components of internal actions and the related generalised sectional deformations. In order to take the pure torsion De Saint Venant capacity into account, the following matrices are introduced

$$\underline{\underline{B}}_{cD0} = G_{c0} I_{cD} \underline{\underline{\kappa}}, \underline{\underline{B}}_{sD} = G_s I_{sD} \underline{\underline{\kappa}} \tag{19}$$

in which $G_{c0}I_{cD}$ and G_sI_{sD} are the De Saint Venant elastic stiffness of concrete slab and steel girder, G_{c0}, G_s are respectively the reference shear modulus of concrete and the shear modulus of steel and $\underline{\underline{\kappa}}$ the diagonal matrix

$$\kappa_{ij} = 0 \ , 1 \le i, j \le 4, \quad i = j \ne 4 \ ; \ \kappa_{44} = 1 \tag{20}$$

Assuming that the Poisson ratio keeps constant in time and introducing internal action vector $\underline{Q}_D^{T\prime} = [0\ 0\ 0\ M_D']$ including pure torsion moment M_D, the equilibrium equation referred to the De Saint Venant capacity results

$$-\underline{Q}_D' = \int_0^t [\underline{\underline{B}}_{cD0} \rho(t, t') + \underline{\underline{B}}_{sD}] d\underline{\Psi} \tag{21}$$

By deriving twice Eq. (16) with respect to the z axis, we obtain

$$\int_0^t [\underline{\underline{B}}_{c0} \rho(t, t') + \underline{\underline{B}}_s^*] d\underline{\Psi}''(z, t') + \underline{\underline{C}}_s \underline{\Psi}_{ls}''(z, t) = \underline{Q}''(z, t) \tag{22}$$

The equilibrium conditions on an infinitesimal strip dz imply

$$N'' = -q_l' \ , \ M_x'' = q_x \ , \ M_y'' = -q_y \ , \ M_t' = -q_\omega \tag{23}$$

where the total torque M_t includes the contribution of warping moment M_ω and pure torsion moment M_D, according to the following relationship

$$M_t = M_\omega' + M_D \tag{24}$$

Introducing Eq. (24) in the last of Eq. (23), the warping moment can be written as

$$M_\omega' = -q_\omega - M_D' \tag{25}$$

Defining vector $\underline{q}$ as

$$\underline{q}^T = [-q_l' \ -q_x \ -q_y \ -q_\omega] \tag{26}$$

according to Eqs. (25), (23), (21), Eq. (22) assumes the form

$$\int_0^t [\underline{\underline{B}}_{c0}\rho(t,t') + \underline{\underline{B}}_s^*]d\underline{\Psi}''(z,t') + \underline{\underline{C}}_s\underline{\Psi}''_{ls}(z,t) - \int_0^t [\underline{\underline{B}}_{cD0}\rho(t,t') + \underline{\underline{B}}_{sD}]d\underline{\Psi}(z,t') = \underline{q}(z,t) \quad (27)$$

Eq. (27) can be inverted by introducing the non-dimensional creep function $\beta(t,t') = J(t,t') / E_{c0}$, in order to obtain

$$\int_0^t [\underline{\underline{B}}_{c0} + \underline{\underline{B}}_s^*\beta(t,t')]d\underline{\Psi}''(z,t') + \underline{\underline{C}}_s\int_0^t d\Psi''_{ls}(z,t')\beta(t,t') - \int_0^t [\underline{\underline{B}}_{cD0} + \underline{\underline{B}}_{sD}\beta(t,t')]d\underline{\Psi}(z,t') = \int_0^t d\underline{q}(z,t')\beta(t,t') \quad (28)$$

The problem can be completely solved by means of the system of 4 integro-differential Eq. (28) and the one of n_s differential Eq. (14).

Regarding the boundary conditions necessary to solve the second order differential Eq. (14), assuming that no axial forces or bending moments are present at the extreme sections of the composite beams, the following relationships have to be satisfied

$$N_s^{(i)}(z_0,t) = 0 \; ; \; N_c(z_0,t) = 0 \; ; \; M_x(z_0,t) = 0 \; ; \; M_y(z_0,t) = 0 \; ; \; M_\omega(z_0,t) = 0, \quad i = 1,\ldots,n_s, \forall t \geq t_0 \quad (29)$$

where z_0 represents the abscissa of the initial and final sections. Hence, from Eq. (16) we obtain

$$\int_0^t [\underline{\underline{B}}_{c0}\rho(t,t') + \underline{\underline{B}}_s^*]d\underline{\Psi}(z_0,t') + \underline{\underline{C}}_s\underline{\Psi}_{ls}(z_0,t) = \underline{Q}(z_0,t) + \int_0^t d\overline{\underline{Q}}_c(t')\rho(t,t') + \overline{\underline{Q}}_s(t) \quad (30)$$

Regarding the first of Eq. (30), each contribution to axial load has to vanish, as indicated in the following relationship

$$E_s[A_s^{(i)}\Psi_{ls}^{(i)}(z_0,t) - S_{sx}^{(i)}\Psi_2(z_0,t) - S_{sy}^{(i)}\Psi_3(z_0,t) - S_{s\omega}^{(i)}\Psi_4(z_0,t)] - \overline{N}_s^{(i)}(t) = 0 \quad (31)$$

$$\int_0^t \{E_{c0}[A_c d\Psi_{lc}(z_0,t') - S_{cx}d\Psi_2(z_0,t') - S_{cy}d\Psi_3(z_0,t') - S_{c\omega}d\Psi_4(z_0,t')] - d\overline{N}_c(t')\}\rho(t,t') = 0$$

In particular, regarding the second of Eq. (31) we can observe that at $t = t_0$, as $\rho(t_0,t_0) = 1$, it results

$$E_{c0}[A_c\Psi_{lc}(z_0,t_0) - S_{cx}\Psi_2(z_0,t_0) - S_{cy}\Psi_3(z_0,t_0) - S_{c\omega}\Psi_4(z_0,t_0)] - \overline{N}_c(t_0) = 0 \quad (32)$$

As $\rho(t,t') > 0 \; \forall \; t, t'$ and the problem has unique solution, the second of Eq. (31) can be expressed in the algebraic form

$$E_{c0}[A_c\Psi_{lc}(z_0,t) - S_{cx}\Psi_2(z_0,t) - S_{cy}\Psi_3(z_0,t) - S_{c\omega}\Psi_4(z_0,t)] - \overline{N}_c(t) = 0 \quad (33)$$

Thus, the axial strains of the steel elements and of the slab can be derived as a function of flexural and torsional curvatures Ψ_2, Ψ_3, Ψ_4 as follows

$$\Psi_{ls}^{(i)}(z_0,t) = \frac{S_{sx}^{(i)}\Psi_2(z_0,t) + S_{sy}^{(i)}\Psi_3(z_0,t) + S_{s\omega}^{(i)}\Psi_4(z_0,t)}{A_s^{(i)}} + \frac{\overline{N}_s^{(i)}(t)}{E_s A_s^{(i)}}$$

$$\Psi_{1c}(z_0, t) = \frac{S_{cx}\Psi_2(z_0, t) + S_{cy}\Psi_3(z_0, t) + S_{c\omega}\Psi_4(z_0, t)}{A_c} + \frac{\bar{N}_c(t)}{E_{c0}A_c} \tag{34}$$

Introducing Eq. (34) in the second, third and fourth equations of system (30), the boundary values of Ψ_2, Ψ_3, Ψ_4 can be finally obtained.

Regarding the initial conditions, substituting $\rho(t_0,t_0) = 1$ in Eq. (27), or $\beta(t_0,t_0) = 1$ in Eq. (28), the equilibrium equations become

$$[\underline{\underline{B}}_{c0} + \underline{\underline{B}}_s^*]\underline{\Psi}''(z, t_0) + \underline{\underline{C}}_s\underline{\Psi}_{1s}''(z, t_0) - [\underline{\underline{B}}_{cD0} + \underline{\underline{B}}_{sD}]\underline{\Psi}(z, t_0) = \underline{q}(z, t_0) \tag{35}$$

and the compatibility Eq. (14) results

$$\underline{\underline{\nu}}\underline{\Psi}''(z, t_0) + \underline{\underline{\mu}}\underline{\Psi}(z, t_0) = -\underline{\underline{\lambda}}\underline{\Psi}_{1s}''(z, t_0) + \underline{\Psi}_{1s}(z, t_0) \tag{36}$$

to which the boundary conditions (34), (30), evaluated at $t = t_0$, have to be assigned.

3. The solution of the problem

In the following some solving methods will be discussed. In particular, three different procedures able to solve the problem in the elastic domain will be associated to an equal number of procedures which can be employed in the long-term analyses. In particular, the elastic closed form solution (CFS) reveals useful when adopting the Age Adjusted Effective Modulus Method (AAEMM) in the viscoelastic domain, the Fourier Series Expansion Method (FSEM) allows to adopt the Reduced Relaxation Function Method (RRFM) and finally the Finite Difference Method (FDM) is useful when solving Volterra integral equations by means of numerical procedures (GM), such as the trapezia rule.

3.1 The elastic solution methods

3.1.1 Closed form solution (CFS)

The closed form solution in the elastic domain can by obtained by solving the following system of n_s second order differential equations in the n_s unknowns $\Psi_{1s}^{(i)}(z, t_0)$

$$\begin{aligned}&[\underline{\underline{\nu}}(\underline{\underline{B}}_{c0} + \underline{\underline{B}}_s^*)^{-1}\underline{\underline{C}}_s - \underline{\underline{\lambda}}]\underline{\Psi}_{1s}''(z, t_0) + [\underline{\underline{\mu}}(\underline{\underline{B}}_{c0} + \underline{\underline{B}}_s^*)^{-1}\underline{\underline{C}}_s + \underline{\underline{I}}]\underline{\Psi}_{1s}(z, t_0) = \\ &= \underline{\underline{\nu}}(\underline{\underline{B}}_{c0} + \underline{\underline{B}}_s^*)^{-1}\underline{Q}''(z, t_0) + \underline{\underline{\mu}}(\underline{\underline{B}}_{c0} + \underline{\underline{B}}_s^*)^{-1}[\underline{Q}(z, t_0) + \underline{\bar{Q}}_c(t_0) + \underline{\bar{Q}}_s(t_0)]\end{aligned} \tag{37}$$

obtained by combining Eq. (16), evaluated at $t = t_0$, with Eq. (36). When evaluated $\Psi_{1s}^{(i)}(z, t_0)$, vector $\underline{\Psi}(z,t_0)$ can be obtained from Eq. (16) as follows

$$\underline{\Psi}(z, t_0) = [\underline{\underline{B}}_{c0} + \underline{\underline{B}}_s^*]^{-1}[\underline{Q}(z, t_0) + \underline{\bar{Q}}_c(t_0) + \underline{\bar{Q}}_s(t_0)] - [\underline{\underline{B}}_{c0} + \underline{\underline{B}}_s^*]^{-1}C_s\underline{\Psi}_{1s}(z, t_0) \tag{38}$$

3.1.2 Fourier Series Expansion Method (FSEM)

As dealing with simply supported beams, the use of the Fourier Series Expansion Method (Tolstov, 1976) is quite profitable. By expanding the imposed deformations, which are constant along the z axis, in Fourier series as follows

$$\bar{\varepsilon}_{c,s}(\ell, z, t_0) = \frac{4\bar{\varepsilon}_{c,s}(\ell, t_0)}{\pi} \sum_{p=1}^{\infty} \delta^{(p)} \frac{\sin \kappa_p z}{p} \tag{39}$$

where $\kappa_p = p\pi/L$, with L span length of the beam, and $\delta^{(p)}=[1-(-1)^p]/2$, and assuming that the end sections are unloaded, it results

$$\underline{\Psi}(0, t_0) = \underline{\Psi}(L, t_0) = \underline{0} \quad , \quad \underline{\Psi}_{ls}(0, t_0) = \underline{\Psi}_{ls}(L, t_0) = \underline{0} \tag{40}$$

Thus, the two vectors of sectional deformations and their derivatives with respect to z can be expanded in sine series, as follows

$$\begin{aligned} \underline{\Psi}(z,t_0) &= \sum_{p=1}^{\infty} \underline{\Psi}_p(t_0) \sin \kappa_p z & \underline{\Psi}_{ls}(z,t_0) &= \sum_{p=1}^{\infty} \underline{\Psi}_{ls,p}(t_0) \sin \kappa_p z \\ \underline{\Psi}''(z,t_0) &= -\sum_{p=1}^{\infty} \kappa_p^2 \underline{\Psi}_p(t_0) \sin \kappa_p z & \underline{\Psi}''_{ls}(z,t_0) &= -\sum_{p=1}^{\infty} \kappa_p^2 \underline{\Psi}_{ls,p}(t_0) \sin \kappa_p z \end{aligned} \tag{42}$$

Introducing Eq. (41) in the compatibility Eq. (36), it results

$$-\underline{\underline{\nu}} \sum_{p=1}^{\infty} \kappa_p^2 \underline{\Psi}_p(t_0) \sin \kappa_p z + \underline{\underline{\mu}} \sum_{p=1}^{\infty} \underline{\Psi}_p(t_0) \sin \kappa_p z = \underline{\underline{\lambda}} \sum_{p=1}^{\infty} \kappa_p^2 \underline{\Psi}_{ls,p}(t_0) \sin \kappa_p z + \sum_{p=1}^{\infty} \underline{\Psi}_{ls,p}(t_0) \sin \kappa_p z \tag{42}$$

Eq. (42) can be written as

$$[\underline{\underline{\mu}} - \kappa_p^2 \underline{\underline{\nu}}] \underline{\Psi}_p(t_0) = [\underline{\underline{I}} + \kappa_p^2 \underline{\underline{\lambda}}] \underline{\Psi}_{ls,p}(t_0) \ , \ p = 1, \ldots, \infty \tag{43}$$

In a similar way, the equilibrium Eq. (35) becomes

$$\begin{aligned} &-[\underline{\underline{B}}_{c0} + \underline{\underline{B}}_s^*] \sum_{p=1}^{\infty} \kappa_p^2 \underline{\Psi}_p(t_0) \sin(\kappa_p z) - \underline{\underline{C}}_s \sum_{p=1}^{\infty} \kappa_p^2 \underline{\Psi}_{ls,p}(t_0) \sin(\kappa_p z) + \\ &-[\underline{\underline{B}}_{cD0} + \underline{\underline{B}}_{sD}] \sum_{p=1}^{\infty} \underline{\Psi}_p(t_0) \sin(\kappa_p z) = \sum_{p=1}^{\infty} \underline{q}_p(t_0) \sin(\kappa_p z) \end{aligned} \tag{44}$$

where the load vector $\underline{q}$ has been expressed in Fourier series as follows

$$\underline{q}(z,t) = \sum_{p=1}^{\infty} \underline{q}_p(t) \sin \kappa_p z \ , \ \underline{q}_p^T = -[-\kappa_p q_{l,p} \quad q_{x,p} \quad q_{y,p} \quad q_{\omega,p}] \tag{45}$$

For $p = 1,\ldots, \infty$ it results

$$[\underline{\underline{B}}_{c0} + \underline{\underline{B}}_{s}^{*}]\kappa_p^2\underline{\Psi}_p(t_0) + \underline{\underline{C}}_s\kappa_p^2\underline{\Psi}_{ls,\,p}(t_0) + [\underline{\underline{B}}_{cD0} + \underline{\underline{B}}_{sD}]\underline{\Psi}_p(t_0) = -\underline{q}_p(t_0) \tag{46}$$

Introducing Eq. (43) in Eq. (46), we obtain

$$\underline{\underline{B}}_p\underline{\Psi}_p(t_0) = -\underline{q}_p(t_0) \quad , \quad p = 1, \ldots, \infty \tag{47}$$

with

$$\underline{\underline{B}}_p = [\underline{\underline{B}}_{c0} + \underline{\underline{B}}_{s}^{*}]\kappa_p^2 + \kappa_p^2\underline{\underline{C}}_s[\underline{\underline{I}} + \underline{\underline{\kappa}}_p^2\underline{\underline{\lambda}}]^{-1}[\underline{\underline{\mu}} - \kappa_p^2\underline{\underline{\nu}}] + [\underline{\underline{B}}_{cD0} + \underline{\underline{B}}_{sD}] \tag{48}$$

Eq. (47) represents ∞ systems of 4 equations, from which $\underline{\Psi}_p(t_0)$ can be immediately derived. The elastic solution $\underline{\Psi}(t_0)$, $\underline{\Psi}_{ls}(t_0)$ can be finally evaluated, according to Eqs. (43), (41).

3.1.3 Finite difference method

When more complex structural schemes or more general load conditions have to be dealt with, numerical solutions of the integro-differential systems have to be performed. For this, let us subdivide the beam axis in m parts $\Delta z_i = z_i - z_{i-1}$. In this way, referring to the i-th section, the compatibility Eq. (36) and the equilibrium Eq. (35) can be written as follows

$$\underline{\underline{\nu}}\frac{\underline{\Psi}_{i-1}^{(l)} - 2\underline{\Psi}_i^{(l)} + \underline{\Psi}_{i+1}^{(l)}}{\Delta z_i^2} + \underline{\underline{\mu}}\underline{\Psi}_i^{(1)} = -\underline{\underline{\lambda}}\frac{\underline{\Psi}_{ls,\,i-1}^{(l)} - 2\underline{\Psi}_{ls,\,i}^{(l)} + \underline{\Psi}_{ls,\,i+1}^{(l)}}{\Delta z_i^2} + \Psi_{ls,\,i}^{(l)} \tag{49}$$

$$[\underline{\underline{B}}_{c0} + \underline{\underline{B}}_{s}^{*}]\frac{\underline{\Psi}_{i-1}^{(l)} - 2\underline{\Psi}_i^{(l)} + \underline{\Psi}_{i+1}^{(l)}}{\Delta z_i^2} + \underline{\underline{C}}_s\frac{\underline{\Psi}_{ls,\,i-1}^{(l)} - 2\underline{\Psi}_{ls,\,i}^{(l)} + \underline{\Psi}_{ls,\,i+1}^{(l)}}{\Delta z_i^2} - [\underline{\underline{B}}_{cD0} + \underline{\underline{B}}_{sD}]\underline{\Psi}_i^{(l)} = \underline{q}_i^{(l)} \tag{50}$$

where $\underline{\Psi}_i^{(l)} = \underline{\Psi}(z_i, t_0)$, $\underline{\Psi}_{ls,\,i}^{(l)} = \underline{\Psi}_{ls}(z_i, t_0)$, $\underline{q}_i^{(l)} = \underline{q}(z_i, t_0)$. By writing eqs. (49), (50) for each section, together with the associated boundary conditions, the elastic solution can be obtained.

3.2. The Viscoelastic solution methods

The long-term behaviour of continuous composite steel–concrete elements subjected to skew bending and torsion can be obtained only by means of numerical algorithms. On the contrary, when dealing with simply supported beams, the general solution of the visco-elastic problem can be derived even by means of Reduced Relaxation Function Method (Mola 1981, 1982, 1986), when previously uncoupled the space problem by means of the Fourier Series Expansion Method. Finally, the closed form solution which can be achieved in the elastic domain can be adopted when approximate constitutive concrete laws are used.

3.2.1 Reduced relaxation functions method

As illustrated at § 3.1.2. for the elastic domain, sectional deformations can be expanded in Fourier series at each time t, as the boundary conditions do not vary in time. Introducing Eq. (41). expressed for a generic time t in the compatibility Eq. (14), for p = 1,…, ∞ it results

$$[\underline{\underline{\mu}} - \kappa_p^2 \underline{\underline{\nu}}]\underline{\Psi}_p(t) = [\underline{\underline{I}} + \kappa_p^2 \underline{\underline{\lambda}}]\underline{\Psi}_{ls,\,p}(t) \tag{51}$$

and the equilibrium Eq. (28) assumes the form

$$\begin{aligned}&\int_0^t [\underline{\underline{B}}_{c0} + \underline{\underline{B}}_s^* \beta(t, t')]\kappa_p^2 d\underline{\Psi}_p(t') + \int_0^t \underline{\underline{C}}_s \kappa_p^2 d\underline{\Psi}_{ls,\,p}(t')\beta(t, t') + \\ &\int_0^t [\underline{\underline{B}}_{cD0} + \underline{\underline{B}}_{sD}\beta(t, t')]d\underline{\Psi}_p(t') = -\int_0^t d\underline{q}_p(t')\beta(t, t'),\ p = 1, \ldots, \infty\end{aligned} \tag{52}$$

Introducing Eq. (51) in Eq. (52), we obtain

$$\begin{aligned}&\int_0^t \{\underline{\underline{B}}_{c0}\kappa_p^2 + \underline{\underline{B}}_{cD0} + [\kappa_p^2 \underline{\underline{B}}_s^* + \kappa_p^2 \underline{\underline{C}}_s (\underline{\underline{I}} + \kappa_p^2 \underline{\underline{\lambda}})^{-1}(\underline{\underline{\mu}} - \kappa_p^2 \underline{\underline{\nu}}) + \underline{\underline{B}}_{sD}]\beta(t, t')\} d\underline{\Psi}_p(t') = \\ &= -\int_0^t d\underline{q}_p(t')\beta(t, t'),\ p = 1, \ldots, \infty\end{aligned} \tag{53}$$

Eq. (53) represents ∞ systems of 4 integral equations. By introducing in Eq. (53). the coupling matrix $\underline{\underline{D}}_p$ defined as

$$\underline{\underline{D}}_p = \underline{\underline{B}}_p^{-1}[\underline{\underline{B}}_{c0}\kappa_p^2 + \underline{\underline{B}}_{cD0}] \tag{54}$$

with $\underline{\underline{B}}_p$ defined in Eq. (48), it results

$$\int_0^t [\underline{\underline{D}}_p + (\underline{\underline{I}} - \underline{\underline{D}}_p)\beta(t, t')]d\underline{\Psi}_p(t') = \int_0^t d\underline{\Psi}_{e,\,p}(t')\beta(t, t'),\ p = 1, \ldots, \infty \tag{55}$$

where

$$\underline{\Psi}_{e,\,p}(t) = -\underline{\underline{B}}_p^{-1}\underline{q}_p(t) \tag{56}$$

It is now possible to uncouple the equation systems (55) by performing the following linear transformation

$$\underline{\Psi}_p = \underline{\underline{K}}_p \underline{\Phi}_p \tag{57}$$

Multiplying Eq. (55) on the left side by $\underline{\underline{K}}_p^{-1}$ and introducing the spectral matrix $\underline{\underline{\Omega}}_p = \underline{\underline{K}}_p^{-1}\underline{\underline{D}}_p\underline{\underline{K}}_p$, Eq. (55) becomes

$$\int_0^t [\underline{\underline{\Omega}}_p + (\underline{\underline{I}} - \underline{\underline{\Omega}}_p)\beta(t, t')]d\underline{\Phi}_p(t') = \int_0^t d\underline{\Phi}_{e,\,p}(t')\beta(t, t') \tag{58}$$

By defining the matrix of the non-dimensional Varied Creep Functions related to the p-th Fourier series as

$$\underline{\underline{\beta}}_p^*(t, t') = \underline{\underline{\Omega}}_p + (\underline{\underline{I}} - \underline{\underline{\Omega}}_p)\beta(t, t') \tag{59}$$

Eq. (58) can be written in the following form

$$\int_0^t \underline{\underline{\beta}}_p^*(t, t')d\underline{\Phi}_p(t') = \int_0^t (\underline{\underline{I}} - \underline{\underline{\Omega}}_p)^{-1}[\underline{\underline{\beta}}_p^*(t, t') - \underline{\underline{\Omega}}_p]d\underline{\Phi}_{e,p}(t') \tag{60}$$

Eq. (60) can be inverted by recurring to the non-dimensional Reduced Relaxation Function matrix, related to the Varied Creep Function one by means of the following integral equation

$$\int_0^t \frac{\partial \underline{\underline{\rho}}_p^*(t', t_0)}{\partial t'} \underline{\underline{\beta}}_p^*(t, t')dt' = \underline{\underline{I}} \tag{61}$$

obtaining

$$\underline{\Phi}_p(t) = \int_0^t (\underline{\underline{I}} - \underline{\underline{\Omega}}_p)^{-1}[\underline{\underline{I}} - \underline{\underline{\Omega}}_p\underline{\underline{\rho}}_p^*(t, t')]d\underline{\Phi}_{e,p}(t') \tag{62}$$

The unknown vector $\underline{\Psi}_p$ can now be derived by remembering Eq. (57)

$$\underline{\Psi}_p(t) = \underline{\underline{K}}_p \int_0^t (\underline{\underline{I}} - \underline{\underline{\Omega}}_p)^{-1}[\underline{\underline{I}} - \underline{\underline{\Omega}}_p\underline{\underline{\rho}}_p^*(t, t')]d\underline{\Phi}_{e,p}(t'), \quad p = 1, \ldots, \infty \tag{63}$$

Introducing Eq. (63) in Eq. (51), it is possible to determine the vector of the longitudinal deformations of the steel beams, related to the p-th terms of the Fourier series. Finally the unknown vectors $\underline{\Psi}$ and $\underline{\Psi}_{1s}$ have to be evaluated by means of Eq. (41).

This way of proceeding is quite profitable when only constant in time loads act on the structure. In fact, by observing Eq. (63), it appears immediately that in the presence of variable loads the evaluation of the term on the right side needs the previous calculation of the Reduced Relaxation Function matrix for each reference time t and for each loading time t′ such that $t_0 \le t' < t$. On the contrary, when the applied loads are constant in time, Eq. (63) assumes the form

$$\underline{\Psi}_p(t) = \underline{\underline{K}}_p(\underline{\underline{I}} - \underline{\underline{\Omega}}_p)^{-1}[\underline{\underline{I}} - \underline{\underline{\Omega}}_p\underline{\underline{\rho}}_p^*(t, t_0)]\underline{\Phi}_{e,p} \tag{64}$$

i.e. the Reduced Relaxation Function matrix has to be determined only referring to loading time t_0.

3.2.2 General method

When more complex structural schemes or more general load conditions have to be dealt with, numerical solutions of the integro-differential systems have to be performed (Bažant 1975, Chiorino, *et al*. 1984). For this, let us subdivide the time domain into n intervals $\Delta t_j = t_j - t_{j-1}$ and let us refer to the beam axis subdivision $\Delta z_i = z_i - z_{i-1}$ introduced at § 3.1.3. In this way, referring to the time $t = t_n$ and to the i-th section, the equilibrium Eq. (28) can be written as follows

$$\frac{\underline{\underline{B}}_c + \underline{\underline{B}}_s^* \beta_{n,n}}{\Delta z_i^2}(\Delta\underline{\Psi}_{i-1}^{(n)} - 2\Delta\underline{\Psi}_i^{(n)} + \Delta\underline{\Psi}_{i+1}^{(n)}) + \sum_{j=1}^{n-1} \frac{\underline{\underline{B}}_c + \underline{\underline{B}}_s^* \beta_{n,j}}{\Delta z_i^2}(\Delta\underline{\Psi}_{i-1}^{(j)} - 2\Delta\underline{\Psi}_i^{(j)} + \Delta\underline{\Psi}_{i+1}^{(j)})$$
$$+ \frac{\underline{\underline{C}}_s}{\Delta z_i^2} \sum_{j=1}^{n} \beta_{n,j}(\Delta\underline{\Psi}_{ls,i-1}^{(j)} - 2\Delta\underline{\Psi}_{ls,i}^{(j)} + \Delta\underline{\Psi}_{ls,i+1}^{(j)}) - \sum_{j=1}^{n} [\underline{\underline{B}}_{cD0} + \underline{\underline{B}}_{sD}\beta_{n,j}]\Delta\underline{\Psi}_i^{(j)} = \sum_{j=1}^{n} \Delta\underline{q}_i^{(j)}\beta_{n,j} \quad (65)$$

with

$$\Delta\underline{\Psi}_i^{(j)} = \underline{\Psi}_i^{(j)} - \underline{\Psi}_i^{(j-1)}, \quad \Delta\underline{\Psi}_{ls,i}^{(j)} = \underline{\Psi}_{ls,i}^{(j)} - \underline{\Psi}_{ls,i}^{(j-1)}, \quad \Delta\underline{q}_i^{(j)} = \underline{q}_i^{(j)} - \underline{q}_i^{(j-1)}, \quad \beta_{n,j} = \frac{\beta(t_n,t_j) + \beta(t_n,t_{j-1})}{2} \quad (66)$$

Referring to the time interval Δt_n, the compatibility Eq. (14) assumes the form

$$\underline{\nu}\frac{\Delta\underline{\Psi}_{i-1}^{(n)} - 2\Delta\underline{\Psi}_i^{(n)} + \Delta\underline{\Psi}_{i+1}^{(n)}}{\Delta z_i^2} + \underline{\underline{\mu}}\Delta\underline{\Psi}_i^{(n)} = -\underline{\underline{\lambda}}\frac{\Delta\underline{\Psi}_{ls,i-1}^{(n)} - 2\Delta\underline{\Psi}_{ls,i}^{(n)} + \Delta\underline{\Psi}_{ls,i+1}^{(n)}}{\Delta z_i^2} + \Delta\underline{\Psi}_{ls,i}^{(n)} \quad (67)$$

By introducing in Eq. (67) the expression of the variation $\Delta\underline{\Psi}_i^{(n)}$ of the unknown vector $\underline{\Psi}_i$ at time $t = t_n$, obtained from Eq. (65) for every section i = 1, …, m as a function of $\Delta\underline{\Psi}_{ls,i}^{(n)}$, the solving system in the unknown vector $\Delta\underline{\Psi}_{ls}^{(n)}$ is obtained. The boundary conditions related to vector $\Delta\underline{\Psi}_{ls,i}^{(n)}$ have to be assigned referring to the 1st and the m-th sections, making the vectors $\Delta\underline{\Psi}_{ls,1}^{(n)}$, $\Delta\underline{\Psi}_{ls,m}^{(n)}$ known terms. Introducing in Eq. (65) the obtained value of $\Delta\underline{\Psi}_{ls}^{(n)}$, vector $\Delta\underline{\Psi}^{(n)}$ can be determined. Finally, by means of Eq. (66), $\underline{\Psi}^{(n)}$, $\underline{\Psi}_{ls}^{(n)}$ can be obtained and the problem is completely solved.

3.2.3 Algebraic method

The solution of the viscoelastic problem can be obtained with a good approximation by adopting the Age Adjusted Effective Modulus Method (AAEMM) as superposition of elastic solutions (Trost 1967, Bažant 1972, Mola and Gatti 1996). In particular, referring to §3.1.1, let us indicate by $\underline{\Psi}_{1s,0}(z,t_0)$, $\underline{\Psi}_0(z,t_0)$ the solution of Eqs. (37),(38) and by $\underline{\Psi}_{1s,1}(z,t)$, $\underline{\Psi}_1(z,t)$, $\underline{\Psi}_{1s,10}(z,t)$, $\underline{\Psi}_{10}(z,t)$ the solutions of the same equations, referred to the reduced modulus $E'_c = E_c/[1 + \chi(t,t_0)\,\varphi(t,t_0)]$, with $\chi(t,t_0)$, $\varphi(t,t_0)$ respectively ageing and creep coefficients, and related to loads at time t and at time t_0, respectively. Introducing the coupling factor $\mu(t,t_0) = -[1 - \chi(t,t_0)] / \chi(t,t_0)$, the final solution can be achieved by means of the following relationship

$$\underline{\Psi}_{1s}(z,t) = \underline{\Psi}_{1s,1}(z,t) + \mu(t,t_0)\,[\underline{\Psi}_{1s,0}(z,t_0) - \underline{\Psi}_{1s,10}(z,t)]\;;\; \underline{\Psi}(z,t) = \underline{\Psi}_1(z,t) + \mu(t,t_0)\,[\underline{\Psi}_0(z,t_0) - \underline{\Psi}_{10}(z,t)] \quad (68)$$

or, in case of constant loads

$$\underline{\Psi}_{1s}(t) = \underline{\Psi}_{1s,1}(t)\,[1 - \mu(t,t_0)] + \mu(t,t_0)\,\underline{\Psi}_{1s,0} \;\;;\;\; \underline{\Psi}(t) = \underline{\Psi}_1(t)\,[1 - \mu(t,t_0)] + \mu(t,t_0)\,\underline{\Psi}_0 \quad (69)$$

4. Case Study

Let us consider the simply supported structure represented in Fig. 5, having the symmetric composite

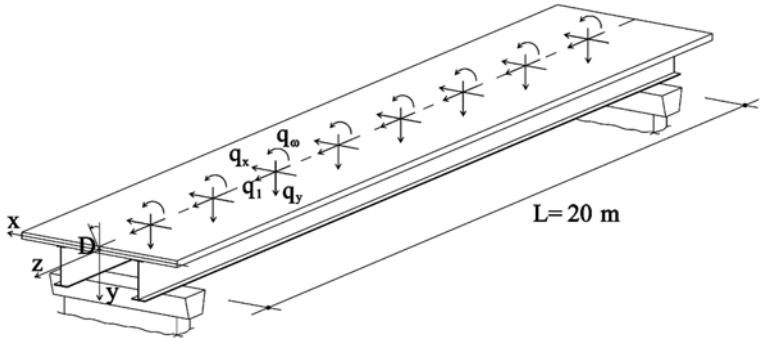

Fig. 5 Structural arrangement

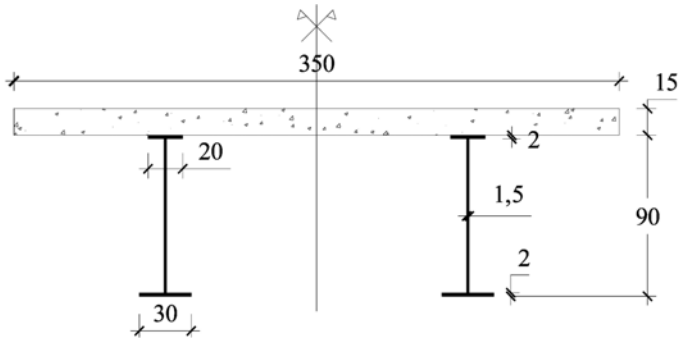

Fig. 6 Transverse section in [cm]

section of Fig. 6. The structure is subjected to uniform distributed loads, constant in time, acting along the reference axes from $t_0 = 28$ days.

The material properties are the following: for the steel beams an elastic modulus $E_s = 210000$ MPa is considered, while for the concrete slab a cylindrical characteristic strength $f_{ck} = 30$ MPa is assumed. The elastic modulus and the creep function are evaluated according to the CEB MC 90 (1993), assuming RH = 70% as environmental humidity. According to the previous assumptions, the concrete elastic modulus at loading age results $E_{c0} = 31977$ MPa, while the ageing and the creep coefficients evaluated at $t_\infty = 30000$ days are respectively $\chi(t_\infty, t_0) = 0.865$, $\varphi(t_\infty, t_0) = 2.068$, from which the coupling factor results $\mu(t_\infty, t_0) = -0.156$. Finally the effective modulus results

$$E'_{c0}(t_\infty, t_0) = \frac{E_{c0}}{1 + \chi(t_\infty, t_0)\varphi(t_\infty, t_0)} = 11464 \text{ MPa}$$

The notional thickness can be evaluated from the geometrical data of Fig. 6, resulting $h_0 = 155$ mm. Regarding the shear connection between the beams and the slab, three different values of the stiffness are considered, namely $k_{ch} = \infty$, $k_{ch} = 3 \cdot 10^5$ kN/m^2, $k_{ch} = 1 \cdot 10^5$ kN/m^2.

The following load conditions will be presented

- Vertical load $q_y = 14$ kN/m, acting on the symmetry axis;
- Transverse load $q_x = 50$ kN/m, acting in the shear centre of the transformed section (13.9 cm above

the slab centroid);

- Torque $q_\omega = 20$ kNm/m.

The solution will be evaluated both according to the RRFM, associated to the FSEM, and by adopting the approximate AAEM Method, associated to the closed form elastic solution.

In the next paragraphs, the diagrams representing the solution of the problem will adopt the following representation

and the stresses in the concrete slab will be multiplied by 10.

4.1. Structure subjected to vertical uniform distributed load q_y

The time evolutions of the Reduced Relaxation Functions are shown in Fig. 7 for the different connections and for the related stiffness ratios ω_m. In case of rigid connectors, the functions are independent on the Fourier series index, while they present increasing values towards the unitary value by increasing both the connector deformability and the series index.

From the elastic solutions, the stiffness parameters ω_m and the Reduced Relaxation Functions, the final values of the axial deformation of the concrete slab can be determined for each term of the series. The initial and final solutions can then be easily obtained by evaluating the Fourier series, e. g. at mid-span the axial strains of the concrete slab are reported in the first columns of Table 1.

From the axial deformation of the slab it is possible to derive the remaining unknowns of the problem: axial deformations $\Psi_{ls}^{(1)} = \Psi_{ls}^{(2)} = \Psi_{ls}$ of the beams and curvature Ψ_3 of the composite section ($\Psi_2 = \Psi_4 = 0$). In particular, at $z = L/2$ the results are reported in Table 1. The differences between the numerical solutions obtained by the RRF and the AAEM Methods are smaller than 5% for all the considered cases.

It is worth noting that the time evolutions of $\Psi_{ls}^{(1)}$, $\Psi_{ls}^{(2)}$ and Ψ_3 can be determined with the RRFM only by solving the integral equation $\int_0^t \rho(t, t')d\Psi_{1c}(t')$ which implies the previous evaluation of the relaxation functions at time t for every time $t' \in [t_0,t]$.

From the results of Table 1, the state of strain and stress of the composite section can be evaluated. They are reported in Fig. 8, Fig. 9, Fig. 10 respectively for $k_{ch} = \infty$, $k_{ch} = 3\times10^5$ kN/m^2, $k_{ch} = 1\times10^5$ kN/m^2. Regarding the elastic deformations, by decreasing the connector stiffness, the slips between the slab and the beams are bigger, producing smaller deformations in the slab but higher strains in the beams, both at the upper and at the lower fibres. The strains increase in time, in a lower extent when increasing the connector deformability, inducing the neutral axis to move downward, producing axial deformations even in the section with rigid connection. It appears worth noting that at initial time the neutral axis coincides with the transformed section centroidal axis, indicated in the diagrams with the dotted line, only in presence of non-deformable connectors. Only in this case the flexural and axial problems result uncoupled.

Regarding the stresses, the connector deformability plays an outstanding role especially in the initial values at the lower fibre of the slab and at the upper fibres of the beams. The marked differences become smaller moving towards the lower beam fibres and the final times.

The deflection diagrams reported in Fig. 11 show the significant influence of the connection system,

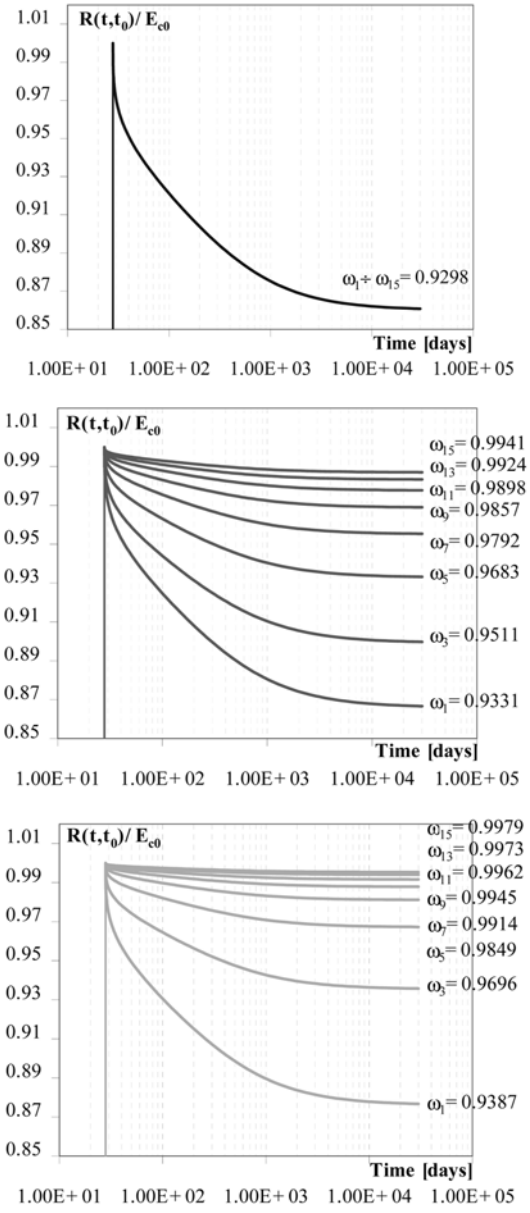

Fig. 7 Reduced Relaxation Functions by varying the connector stiffness

to which an increase of the displacements of more than 50% is related, when considering the extreme stiffness values. According to the previous results, the time increases move from 55% in the case of rigid connection to 30% when considering the connector deformability.

4.2 Structure subjected to horizontal uniform distributed load q_x through the shear centre

The time evolutions of the Reduced Relaxation Functions are represented in Fig. 12.

Table 1. Initial and final values of the axial strain of the slab and the beam and of the section curvature

	Ψ_{1c} (L/2,t)				Ψ_{1s} (L/2,t)				Ψ_{1s} (L/2,t)			
k_{ch} [kN/m^2]	$t = t_0$	$t = t_\infty$ RRF	$t = t_\infty$ AAEM	error	$t=t_0$	$t = t_\infty$ RRF	$t = t_\infty$ AAEM	error	$t=t_0$	$t = t_\infty$ RRF	$t = t_\infty$ AAEM	error
∞	-7.04×10^{-5}	-2.00×10^{-4}	-1.91×10^{-4}	4.8%	-7.04×10^{-5}	-2.00×10^{-4}	-1.91×10^{-4}	4.6%	-4.04×10^{-4}	-6.39×10^{-4}	-6.22×10^{-4}	2.6%
3×10^5	-6.76×10^{-5}	-1.93×10^{-4}	-1.84×10^{-4}	4.8%	-1.07×10^{-4}	-2.27×10^{-4}	-2.18×10^{-4}	4.0%	-4.70×10^{-4}	-6.88×10^{-4}	-6.72×10^{-4}	2.4%
1×10^5	-6.23×10^{-5}	-1.80×10^{-4}	-1.71×10^{-4}	4.8%	-1.76×10^{-4}	-2.79×10^{-4}	-2.72×10^{-4}	2.6%	-5.96×10^{-4}	-7.82×10^{-4}	-7.69×10^{-4}	1.7%

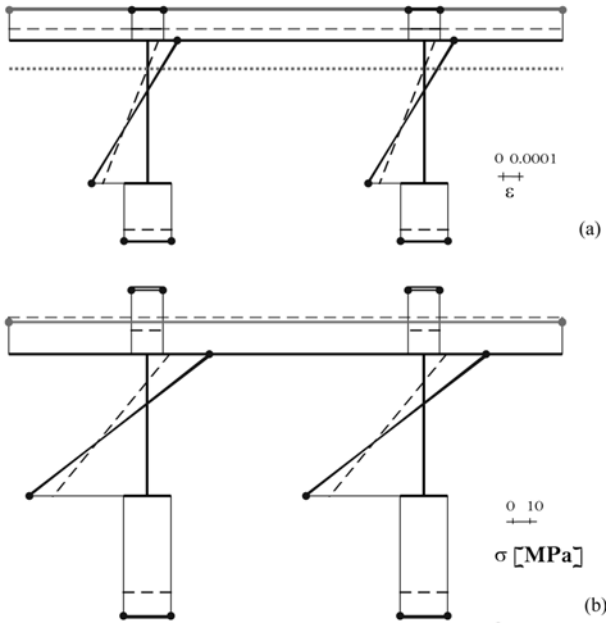

Fig. 8 Strains (a) and stresses (b) at initial and final time, with $k_{ch} = \infty$

In case of rigid connection, the Reduced Relaxation Function is lower than the one related to vertical loads, indicating greater creep effects. This fact is due to the greater stiffness of the steel element with respect to the concrete part, resulting in a smaller stiffness ratio, when the composite structure is subjected to bending moments M_x.

From the previous results, the final values of the curvature in the z-x plane can be determined for each term of the series. The initial and final solutions in terms of curvature in the z-x plane, axial deformation of the steel beam and torsional curvature at mid-span are reported in Table 2, together with the errors between the RRF and the AAEM solutions.

The sectional strains and stresses of the mid-span section are reported in Fig. 13, Fig. 14 for $k_{ch} = \infty$, $k_{ch} = 3 \times 10^5$ kN/m^2. Referring to the strain diagrams of the section with rigid connection and especially observing the web deformations, the creep effect in coupling the flexural and torsional behaviour is clearly visible.

In the elastic domain the neutral axis of the plane strain distribution connected to the bending moment M_x coincides with the y axis, while the section loses its planarity in time owing to the growth of

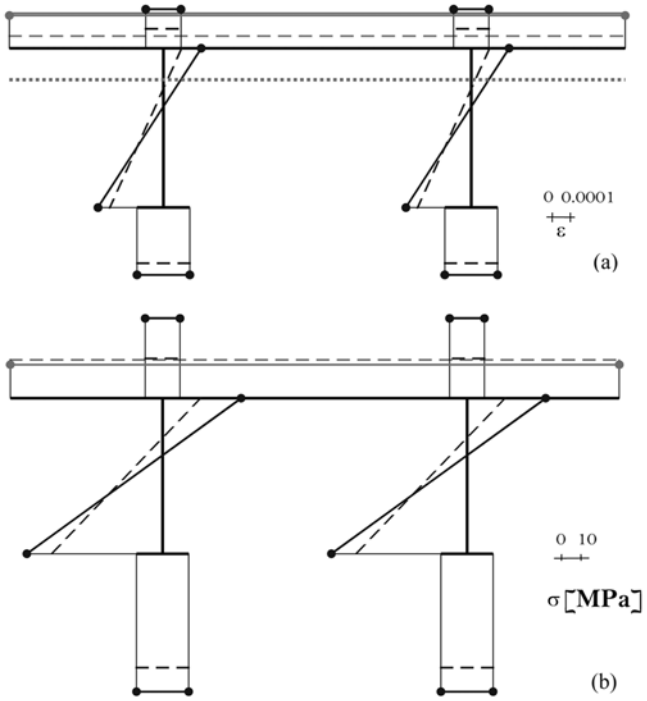

Fig. 9 Strains (a) and stresses (b) at initial and final time, with $k_{ch} = 3 \times 10^5$ kN/m^2

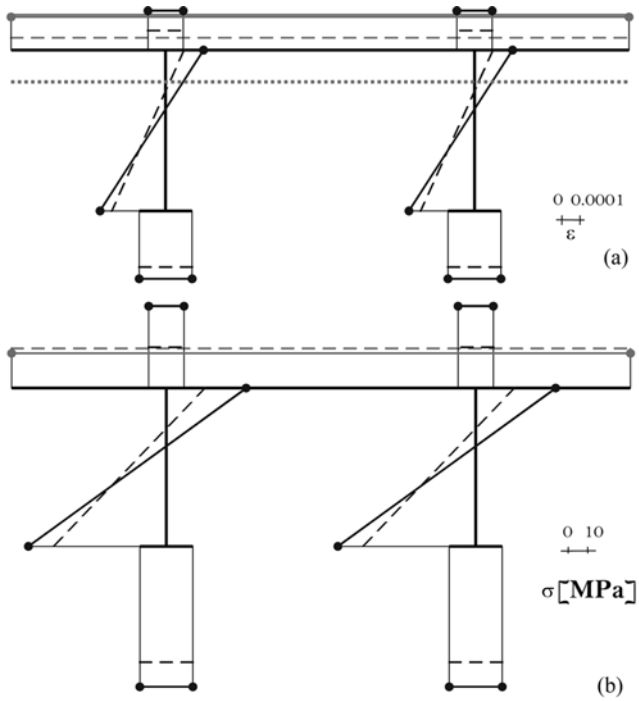

Fig. 10 Strains (a) and stresses (b) at initial and final time, with $k_{ch} = 1 \times 10^5$ kN/m^2

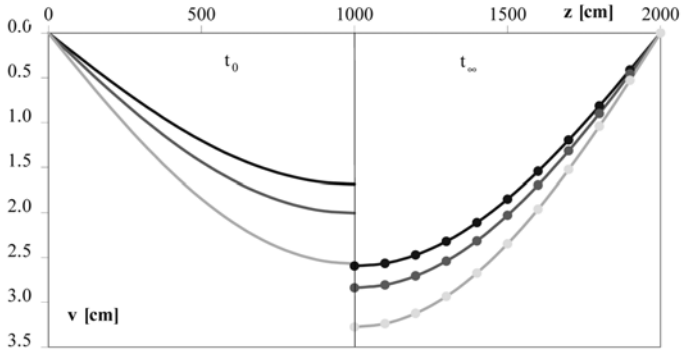

Fig. 11 Displacements of the beam axis in the y direction at initial and final time, by varying the connector stiffness

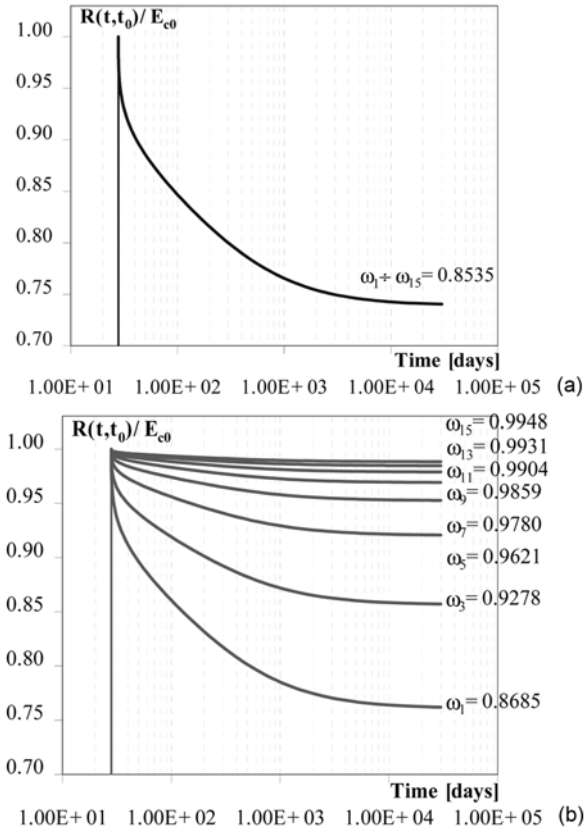

Fig. 12 Reduced Relaxation Functions for $k_{ch} = \infty$ (a), $k_{ch} = 3\times10^5$ kN/m^2 (b)

warping strains. This can be explained by considering that at initial time the horizontal force acting in the shear centre only produces flexural effects, while a negative torque contribution increasing in time has to be added due to the upward translation of the shear centre.

Otherwise, when deformable connectors are considered, the state of deformation is not plane even at

Table. 2 Initial and final values of the curvature in the z-x plane, of the axial strain of the beams and of the torsional curvature

	Ψ_2 (L/2,t) [m^{-1}]				Ψ_{1s} (L/2,t)				Ψ_4 (L/2,t) [m^{-2}]			
k_{ch} [kN/m^2]	$t = t_0$	$t = t_\infty$ RRF	$t = t_\infty$ AAEM	error	$t = t_0$	$t = t_\infty$ RRF	$t = t_\infty$ AAEM	error	$t = t_0$	$t = t_\infty$ RRF	$t = t_\infty$ AAEM	error
∞	-1.02×10^{-4}	-2.56×10^{-4}	-2.44×10^{-4}	4.5%	0.00	-6.25×10^{-8}	0.00	-	0.00	2.01×10^{-5}	1.86×10^{-5}	7.5%
3×10^5	-1.06×10^{-4}	-2.72×10^{-4}	-2.60×10^{-4}	4.6%	-2.80×10^{-5}	-4.41×10^{-5}	-4.28×10^{-5}	2.9%	-3.82×10^{-6}	1.54×10^{-5}	1.39×10^{-5}	9.3%

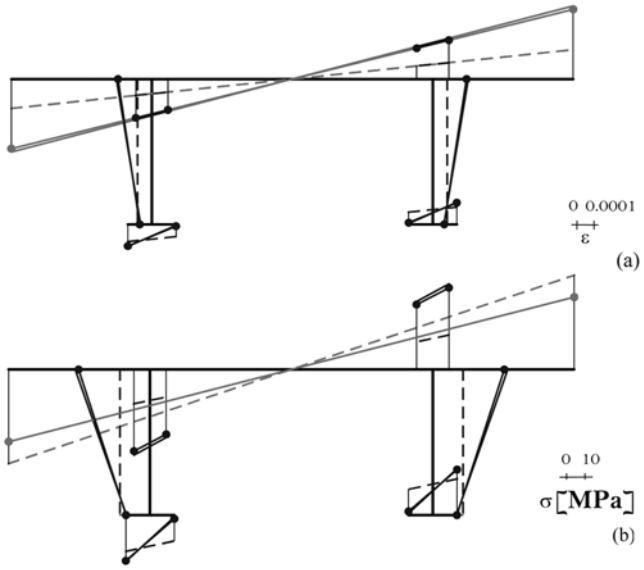

Fig. 13 Strains (a) and stresses (b) at initial and final time, with $k_{ch} = \infty$

loading time. This occurs as point D where the load is applied cannot be considered any more as the shear centre of the composite section due to the introduction of strain discontinuities within the cross section.

The stresses are highly influenced by the sectional redistribution due to the viscoelastic behaviour of the slab, showing a marked increase especially in the upper flanges. Even the stress distribution presents the out of plane component related to warping torsion.

The displacements of the longitudinal axis in the x direction reported in Fig. 15 show interesting aspects. First of all, as no slip in the transverse direction is allowed, the very small differences related to the connector stiffness present both at initial and at final time are a consequence of the warping deformations acting in the longitudinal direction. Furthermore, the final displacements are about 150% with respect to the initial ones. This value is greater than the one connected to the vertical load, which was between 30% and 55%. This result is connected to the lower values of the Reduced Relaxation Functions reported in Fig. 12, due to the lower steel–concrete stiffness ratio.

Regarding the secondary effects of the horizontal loads, the rotations around the z axis are shown in Fig. 16. According to the previous discussion, at initial time the section with rigid connectors does not present any rotation. On the contrary, it assumes in time non zero values. In the case of deformable

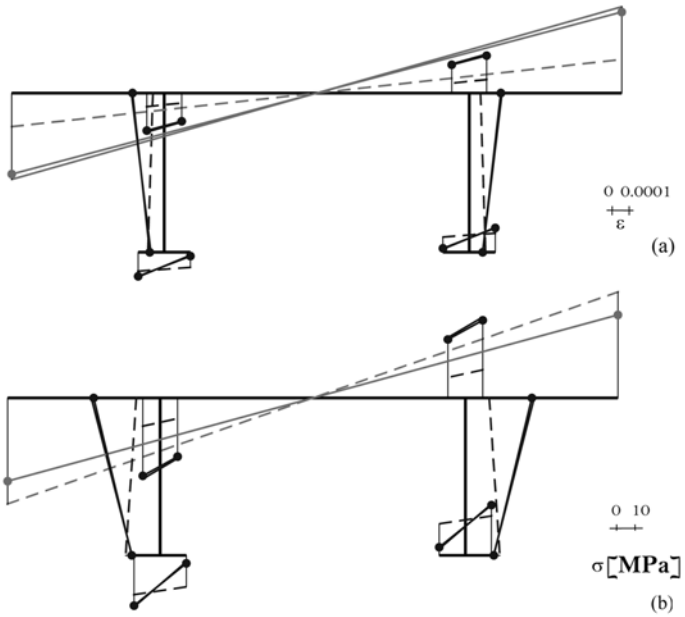

Fig. 14 Strains (a) and stresses (b) at initial and final time, with $k_{ch} = 3\times10^5$ kN/m^2

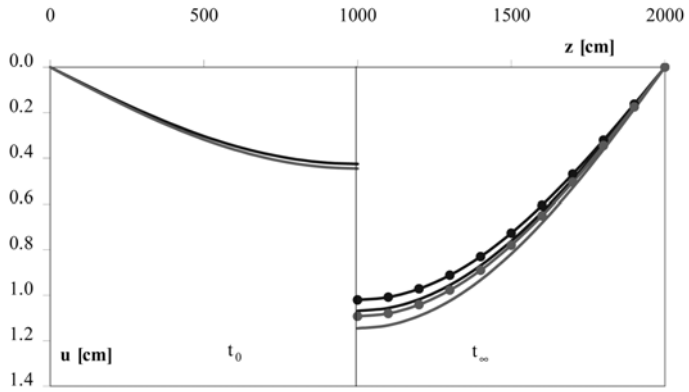

Fig. 15 Displacements of the beam axis in the x direction at initial and final time, with $k_{ch} = \infty$, $k_{ch} = 3\times10^5$ kN/m^2

connectors, the rotations which are already present in the elastic domain change sign in time. This fact can occur because the force is applied in the shear centre of the rigid section, which does not have a physical meaning when the transverse section presents discontinuities in terms of strains and displacements.

4.3 Structure subjected to uniform distributed torque q_ω

The initial and final solutions in terms of curvature in the z-x plane, axial deformation of the steel beam and torsional curvature at mid-span are reported in Table 3.

The states of strains and stresses reported in Fig. 17, Fig. 18 present dual characteristics with respect to the case of horizontal load. In fact, in presence of rigid connection, the elastic strains have the same

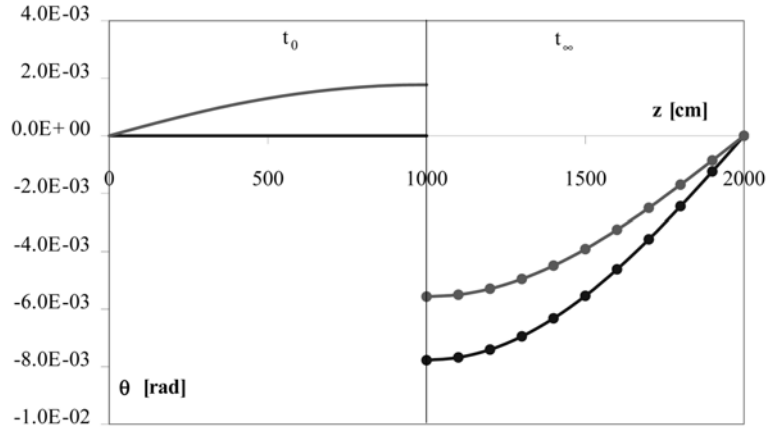

Fig. 16 Rotation of the beam axis around the z axis at initial and final time, with $k_{ch} = \infty$, $k_{ch} = 3\times10^5$ kN/m^2

Table. 3 Initial and final values of the curvature in the z-x plane, of the axial strain of the beam and of the torsional curvature

	Ψ_2 (L/2,t) [m^{-1}]				Ψ_{1s} (L/2,t)				Ψ_4 (L/2,t) [m^{-2}]			
k_{ch} [kN/m^2]	$t=t_0$	$t=t_\infty$ RRF	$t=t_\infty$ AAEM	error	$t=t_0$	$t=t_\infty$ RRF	$t=t_\infty$ AAEM	error	$t=t_0$	$t=t_\infty$ RRF	$t=t_\infty$ AAEM	error
∞	6.51×10^{-5}	1.63×10^{-4}	1.56×10^{-4}	4.5%	0.00	3.99×10^{-8}	0.00	-	-4.69×10^{-5}	-5.97×10^{-5}	-5.88×10^{-5}	1.6%
3×10^5	5.82×10^{-5}	1.50×10^{-4}	1.43×10^{-4}	4.6%	-4.45×10^{-5}	-3.49×10^{-5}	-3.57×10^{-5}	2.2%	-5.30×10^{-5}	-6.34×10^{-5}	-6.26×10^{-5}	1.2%

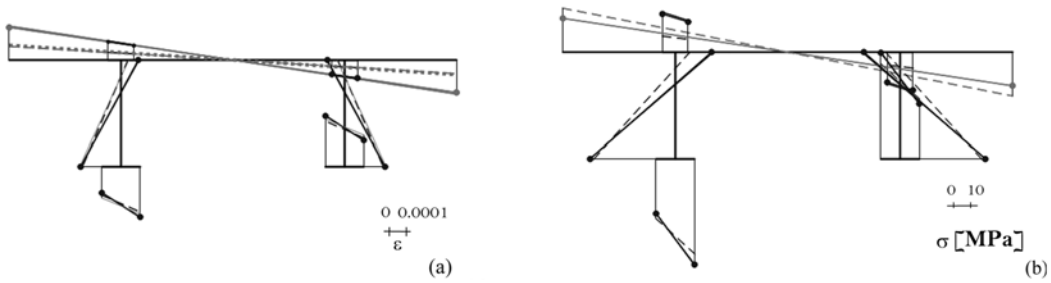

Fig. 17 Strains (a) and stresses (b) at initial and final time, with $k_{ch} = \infty$

distribution as the sectorial area ω, represented by the dotted line. In all the other cases the strains and the coordinate ω present some differences, connected to the coupling between the torsional and the flexural problems.

The stresses present the typical warping distribution, to which the bending stresses have to be added in the final configuration. The influence of the connector deformability prevails in the zone near the steel–concrete interface.

The rotations around the z axis and the horizontal displacements are shown respectively in Figs. 19 and 20.

In both cases the connector stiffness determines only the warping contributions, as the transverse deformability of the connection system has been neglected in each case. The rotations present a low

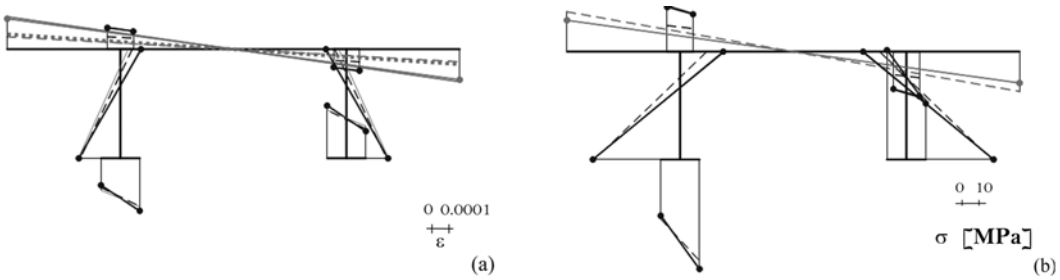

Fig. 18 Strains (a) and stresses (b) at initial and final time, with $k_{ch} = 3\times10^5$ kN/m^2

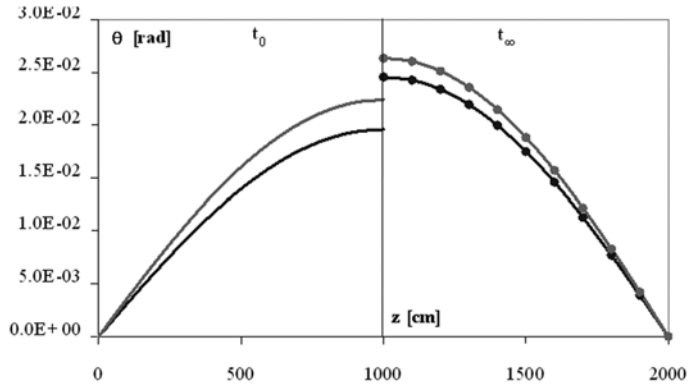

Fig. 19 Rotation of the beam axis around the z axis at initial and final time, with $k_{ch} = \infty$, $k_{ch} = 3\times10^5$ kN/m^2

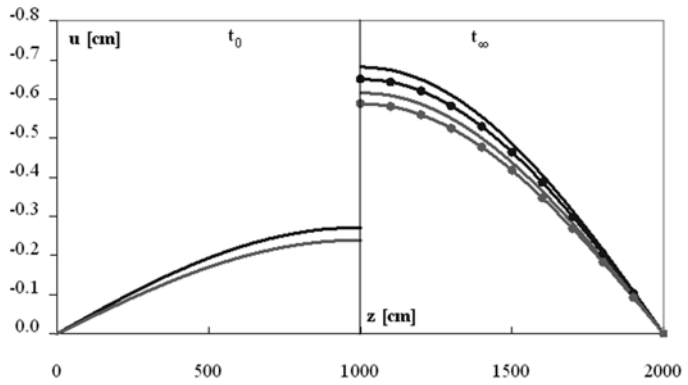

Fig. 20 Displacements of the beam axis in the x direction at initial and final time, with $k_{ch} = \infty$, $k_{ch} = 3\times10^5$ kN/m^2

time increment, due to the coupling between flexural and torsional problems.

On the contrary, horizontal deflections increase of about 150% as in the previous case, as the response is governed by the same Reduced Relaxation Functions. The initial values are not zero both for the rigid and for the deformable connections because they are referred to the reference system origin which does not coincide with the shear centre.

5. Conclusions

The long-term analysis of simply supported composite steel–concrete bridge beams with thin-walled open cross section subjected to skew bending and torsion has been presented. The warping of the transverse sections and the longitudinal slip at the interface between the steel beams and the concrete slab have been considered in the analysis, by adopting the sectorial areas theory.

Interesting results have been derived both by numerically solving the integro-differential equations governing the problem and by adopting approximate methods, showing good agreement between the solutions. In particular, concrete creep induces a coupling between the flexural and torsional problems. The treatment presented provides accurate information about the service stage behaviour of composite beams, highlighting the contribution of the different structural parts (steel and concrete elements) in the time evolution of the structural response in terms of strains and stresses.

The formulation could be extended by introducing non-linearity of the materials (i.e. concrete cracking) and by considering redundant static schemes. In this regard, please note that when non-symmetric cross-section are dealt with, due to the deferred deformation of concrete, the reactions of the supports produce torsional effects over time in addition to the bending ones already present in the elastic phase.

References

Amadio, C. and Fragiacomo, M. (1997), "Simplified Approach to Evaluate Creep and Shrinkage Effects in Steel-Concrete Composite Beams", *J. Struct. Eng.* ASCE, **123**(9), 1153-1164.

Ayoub, A. (2005), "A force-based model for composite steel-concrete beams with partial interaction", *J. Constr. Steel Res*., **61**(3), 387-414.

Ayoub, A.S. and Filippou, F.C. (2000), "Mixed formulation of nonlinear steel-concrete composite beam element", *J. Struct. Eng.* ASCE, **126**(3), 371-381.

Bažant, Z.P. (1972), "Prediction of Concrete Creep Effects using Age-Adjusted Effective Modulus Method", *ACI J.*, **69**(4), 212-217.

Bažant, S.P. (1975), *Theory of Creep and Shrinkage in Concrete Structures; A Precis of Recent Developments*, Mechanics Today, 2, Pergamon Press.

Bradford, M.A. and Gilbert, R.I. (1992), "Composite Beams with Partial Interaction under Sustained Loads", *J. Struct. Eng*. ASCE, **118**(7), 1871-1883.

CEBFIP (1993), *Model Code 1990, Design Code*, Thomas Telford, London.

Chapman, J.C., Dowling, P.J., Lim, P.T.K. and Billington, C.J. (1971), "The Structural Behaviour of Steel and Concrete Box Girder Bridges", *Struct. Eng*., **49**(3), 111-120.

Chiorino, M.A., Koprna, M., Mola, F. and Napoli, P. (1984), *CEB-FIP Manual on Structural Effects of Time Dependent Behaviour of Concrete*, CEB Bulletin d'Information no. 142-142bis, Georgi, St. Saphorin, CH.

Colville, J. (1973), "Tests of Curved Steel-Concrete Composite Beams", *Journal of the Structural Division*, **99**(7), 1555-1570.

Dall'Asta, A. and Zona, A. (2004), "Comparison and validation of displacement and mixed elements for the nonlinear analysis of continuous composite beams", *Comput. Struct.*, **82**(23-26), 2117-2130.

De Miranda, F. (1961), "Comportamento statico sotto azioni torcenti di ponti a travata in sistema misto acciaio-calcestruzzo", *Conf. at Università di Pisa*, (Extracted from Costruzioni Metalliche, No. 4, 1961) (in Italian).

Fragiacomo, M., Amadio, C. and Macorini, L. (2004), "Finite-Element Model for Collapse and Long-Term Analysis of Steel-Concrete Composite Beams", *J. Struct. Eng*. ASCE, **130**(3), 489-497.

Giussani, F. (2004), "Stresses and Deformations in Composite Steel-Concrete Elements with Deformable Connectors Subjected to Sustained Loads", PhD Thesis, Politecnico di Milano, Italy.

Giussani, F. and Mola, F. (2009), "The displacement method for the long-term analysis of steel-concrete beams

with flexible connection", *J. Struct. Eng*., submitted for acceptance.
Kim, K. and Yoo, C.H. (2006a), "Effects of external bracing on horizontally curved box girder bridges during construction", *Eng. Struct*., **28**(12), 1650-1657.
Kim, K. and Yoo, C.H. (2006b), "Steel Concrete Composite Trapezoidal Box Girders in Positive Bending", *Adv. Struct. Eng*., **9**(5), 707-718.
Kolbrunner, C.F. and Basler, K. (1969), *Torsion in Structures, Springer-Verlag Berlin Heidelberg*, New York.
Kwak, H.G. and Seo, Y.J. (2002), "Time-dependent behavior of composite beams with flexible connectors", *Comput. Methods Appl. M*., **191**(34), 3751-3772.
Limkatanyu, S. and Spacone, E. (2002), "Reinforced concrete frame element with bond interfaces. II: state determinations and numerical validation", *J. Struct. Eng*.ASCE, **128**(3), 356-364.
McHenry, D.(1943), "A New Aspect of Creep in Concrete and its Applications to Design", *Proc. ASTM*, 1069-1087.
Mola, F. (1981), "Il Metodo delle Funzioni di Rilassamento Ridotte nella Risoluzione di Strutture Elastoviscose non Omogenee a Modulo Elastico Variabile nel Tempo", Studi e Ricerche, Italcementi, Bergamo, **3** (in Italian).
Mola, F. (1982), "Applicazione del Metodo delle Funzioni di Rilassamento Ridotte all'Analisi di Strutture Viscoelastiche non Omogenee", Studi e Ricerche, Italcementi, Bergamo, **4** (in Italian).
Mola, F. (1986), "Analisi generale in fase viscoelastica lineare di strutture e sezioni a comportamento reologico non omogeneo", Studi e Ricerche, Italcementi, Bergamo, **8**, 119-196, (in Italian).
Mola, F. (1994), "Creep Analysis of Composite Steel-Concrete Members with Deformable Connectors", *ASCE Structures Congress XII*, Atlanta, 2095-2111.
Mola, F. and Gatti, M. (1996), "General and Approximate Approach for the Analysis of Composite Steel-Concrete Members with Deformable Connectors", Studi e Ricerche, Italcementi, Bergamo, **17**, 69-98.
Mola, F. and Giussani, F. (2003), "Service Stage Behaviour of Composite Bridges", *III Int. Conf. on New Dimensions in Bridges*, Kuala Lumpur, Malaysia, April 9-10, 45-62.
Nakamura, S., Momiyama, Y., Hosaka, T. and Homma, K. (2002), "New technologies of steel concrete composite Bridges", *J. Constr. Steel Res*., **58**(1), 99-130.
Newmark, N.M., Siess, C.P. and Viest, I.M. (1951), "Tests and Analysis of Composite Beams with Incomplete Interaction", *Proc. of Society for Experimental Stress Analysis*, **9**, 75-92.
Ng, S.F., Cheung, M.S. and Hachem, H.M. (1993), "Study of a Curved Continuous Composite Box Girder Bridge", *Can. J. Civil Eng*., **20**(1), 107-119.
Rodriguez-Gutierrez, J.A. and Aristizabal-Ochoa, J.D. (2007), "Short- and Long-Term Deflections in Reinforced, Prestressed, and Composite Concrete Beams", *J. Struct. Eng*. ASCE, **133**(4), 495-506.
Sennah, K. and Kennedy, J.B. (1999), "Simply Supported Curved Cellular Bridges: Simplified Design Method", *J. Bridge Eng*., **4**(2), 85-94.
Simo, J.C. and Vu-Quoc, L. (1991), "A Geometrically-Exact Rod Model Incorporating Shear and Torsion-Warping Deformation", *Int. J. Solids Struct*., **27**(3), 371-393.
Thevendran, V., Chen, S., Shanmugam, N.E. and Liew, J.Y.R. (1999), "Nonlinear analysis of steel-concrete composite beams curved in plan", *Finite Elem. Anal. Des*., **32**(3), 125-139.
Thevendran, V., Shanmugam, N.E., Chen, S. and Liew, J.Y.R. (2000), "Experimental Study on Steel-Concrete Composite Beams Curved in Plan", *Eng. Struct*., **22**(8), 877-889.
Tolstov, G.P. (1976), *Fourier Series*, Dover Publications Inc., New York.
Topkaya, C. and Williamson, E.B. (2003), "Development of computational software for analysis of curved girders under construction loads", *Comput. Struct.*, **81**(21), 2087-2098.
Trost, H. (1967), "Auswirkungen des Superpositionsprinzips auf Kriech- und Relaxationsprobleme bei Beton und Spannbeton", *Beton und Stahlbetonbau*, **10**, 230-238, **11**, 261-269.
Turkstra, C.J. and Fam, A.R.M. (1978), "Behaviour Study of Curved Box Bridges", *Journal of the Structural Division*, **104**(3), 453-462.
Virtuoso, F. and Vieira, R. (2004), "Time dependent behaviour of continuous composite beams with flexible connection", *J. Constr. Steel Res*., **60**(3-5), 451-463.
Vlasov, V.Z. (1962), *Pieces Longues en Voiles Minces*, Eyrolles, Paris.

CC